RSC Advances

ROYAL SOCIETY OF CHEMISTRY

www.rsc.org/advances

Tunable Composite Architecture and Homogeneous Dispersion of Charged SiO_2 in Polymer Matrix Assisted by Poly(2-Ethylhexyl acrylate) (P2EHA) Latex Prepared by Self-Assembly through Electrostatic Interaction

Zheng Su[a], Hua Wang[a, *], Fei Xu[a], Konghu Tian[a], Jingwei Wu[b], Xingyou Tian[a, **]

[a] Technology and Engineering Research Center of Advanced Materials, Institute of Applied Technology, Hefei Institutes of Physical Science, C.A.S, No 2221, West Changjiang Road, Hefei, Anhui, P. R. China CN 230088.

[b] Department of Chemical Engineering and Life Science, Wuhan University of Technology, 122 Luoshi Road,Wuhan,Hubei, P.R.China CN 430070.

[*] Corresponding author 1, Tel.: +86 130 33808 1113; E-mail: wanghua@issp.ac.cn.

[**] Corresponding author 2, Tel.: +86 551 65591418; E-mail: xytian@issp.ac.cn.

Abstract: We report a simple and environmentally friendly approach for preparing homogeneous dispersion poly(2-ethylhexyl acrylate)-silicon dioxide (P2EHA-SiO_2) composites by self-assembly of negatively charged P2EHA and charged SiO_2. The P2EHA latex particles were prepared by miniemulsion polymerization using the free-radical initiator. As auxiliary monomer, acrylic acid created the positive charges on the surface of the P2EHA latex. By mixing P2EHA latex particles with positively charged SiO_2 ($pSiO_2$) particles, negatively charged P2EHA latex particles easily assembled with $pSiO_2$ particles through electrostatic interaction. The presence of

P2EHA latex particles assisted the homogeneous dispersion of $pSiO_2$ particles in polymer matrix. After film formation process, the film exhibited excellent thermal-tolerance and adhesive properties. A three-component system of P2EHA latex particles, $pSiO_2$, and negatively charged SiO_2 ($nSiO_2$) were also achieved successfully due to the mutual assistance effect. A better thermal-tolerance and adhesive properties we obtained. Through the establishment of the film formation mechanism, we found that the architecture of the composite film has a significant influence on thermal-tolerance and adhesive properties. This composite material have great application potential on PSA (pressure sensitive adhesive). Our research demonstrates the excellent composite system and provide a convenient approach to realize a wide range of multifunctional fillers and compatible with processing on flexible polymer substrates.

Keywords: composite materials, Polymer-matrix composites (PMCs), Synergism, Modeling

1. Introduction

For a high effective pressure sensitive adhesive (PSA), a balance of cohesive resistance and dissipative properties is needed. Cohesive resistance is normally controlled by the cross-linking or rigid filler of the polymer matrix. However, because of the highly viscoelastic to resist detachment from a surface is also required, the design of a PSA focuses on how to achieve the optimum compromise between these two conflicting properties.[1]

Organic/inorganic composite materials had been studied extensively for a long

time. The advantages of the inorganic material (e.g., rigidity, thermal stability) and the organic polymer (e.g., ductility, dielectric, flexibility, and processability) were combined by them. Moreover, they usually contain special properties of fillers leading to the improvement of material properties.[2-6] Polymer-silica composites had attracted substantial and industrial interest which were the most commonly reported in the literature. They had received much attention in recent years and had been employed in variety of application, such as stimuli-responsive materials,[7-9] superhydrophobic surface,[10] decorative and protective coating,[11] dental materials,[12] flame-retardant materials,[13, 14] and optical devices.[15-17]

From the health and environmental point of view, water borne polymer materials were preferred in most circumstances due to their lower volatile organic compound (VOC) content compared with solvent-borne products.[18] However, the utility of aqueous based composite materials were restricted to some extent due to their inferior properties, such low mechanical strength, thermal stability and water resistance.[19-21] In order to improve the properties mentioned above, Many and significant attempts had been carried out during the last decade.[22-26] It was worth mentioning that colloidal blending based on latex technology has been widely used to prepare composite materials.[27, 28] This latex route has two major advantages as compared to the solution route or melt route. First, this synthetic route is sustainable due to the latex which made in an aqueous suspension without using organic solvent. Second, in this technique, the polymer latex particles create excluded volume and push nanofiller particles into the interstitial space between them essentially, reducing the space available for the filler dramatically to form

a segregated network.

In this present work, we focus on a specific strategy to design the structure of the composite materials film and taking advantage of the film formation mechanism from composite particles. We first used AA as the auxiliary monomer and synthesized the long-stable P2EHA latex particles via a miniemulsion polymerization. Well-dispersed composite particles prepared by mixing the P2EHA latex particles and charged SiO_2 (positively charged SiO_2 particles and negatively charged SiO_2) through electrostatic interaction via colloidal blending technology. The excellent dispersion of SiO_2 particles in polymer matrix due to the interaction between the latex particles and the SiO_2 particles. The film formation mechanism of the composite materials was proposed to investigate the relationship between morphology of composite particles and the composite film architecture.

2. Experimental Section

2.1 Materials

2-Ethylhexyl acrylate (2EHA) (Aladdin Reagents (Shanghai,China)) and acrylic acid (AA) (Sinopharm Chemical Reagent (Beijing,China)) were purified via column chromatography over Al_2O_3. Neutral SiO_2, $pSiO_2$ (positively charged SiO_2) and $nSiO_2$ (negatively charged SiO_2) purchased from Shanghai Dike industrial Co., LTD. Sodium dodecyl sulfate (SDS) and octylphenylpolyethylene glycol (Triton X-100) (Aladdin Reagents (Shanghai,China)) were used as emulsifier. 2,2'-Azobis(2-methylpropionitrile (AIBN) (Sinopharm Chemical Reagent (Beijing,China)) was used as initiator. Phosphotungstic acid hydrate (AR, Aladdin Industrial Corporation) was used to dye the

sample in TEM testing. Ammonia (Sinopharm Chemical Reagent (Beijing,China)) was used to adjust the pH of the latex after the reaction ends. Deionized-water was used for the all experiments. Except monomers, all chemicals were used as received without further purification.

2.2 Preparation of Miniemulsion

The miniemulsions were prepared as follow. 0.63g SDS/Triton X-100 emulsifiers were dissolved in water to prepare the aqueous phase, and all the monomers (2EHA: 20.70g; AA: 0.90g) and initiator (0.13g) were mixed to prepare the oil phase. As we all know that in order to avoid the Ostwald ripening effect, a costabilizer is needed. In general, the costabilizer is a low molecular weight highly water-insoluble compound, but it is unreactive and hence it will increase the volatile organic compound (VOC) content of the final latex. Therefore, in this work, the reactive monomer 2-ethylhexyl acrylate was used to minimize the Ostwald ripening effect at the same time. As it is incorporated into the polymer, it does not increase the VOC content of latex. The aqueous phase and the oil phase were added to a 250mL glass jacketed reactor fitted with a N_2 inlet and a tetrafluoroethylene impeller rotating at 1500 rpm for 30 min. The theoretical solid content of the miniemulsion was about 45 wt%.

2.3 Preparation of Negatively Charged P2EHA latex

The continuous miniemulsion polymerization was carried out at a 250 mL glass jacketed reactor fitted with a reflux condenser, a sampling device, a N_2 inlet, a feeding inlet a tetrafluoroethylene anchor stirred equipped with two blade impellers rotating at 200 rpm. The reaction was carried out at 70 °C for 3 h, protected from light during the

reaction. The latex was then cooled to below 30 °C, filtered through a 30 mesh strainer to remove the emulsion particle agglomerated and charged SiO_2 which unstable in the aqueous phase then ammonia was added to adjust the pH to about 7~8.

2.4 Preparation of P2EHA-pSiO_2 and P2EHA-pSiO_2/nSiO_2 Composite Particle

Various amount of pSiO_2 or nSiO_2 were solved in 5 mL deionized water with the help of the ultrasonic and the magnetic stirring, ‘‘phm’’ is the abbreviation for ‘‘parts per hundred parts monomer. The dispersion of charged SiO_2 was dropped into the P2EHA latex within 10 seconds when the reaction proceeds at the time of 150 min. Subsequently, the P2EHA latex and charged SiO_2 would be mixed with the temperature of 70 °C for 30min.

All experiments were coded as P2EHA-pSiO_2-X or P2EHA-pSiO_2/nSiO_2-Y (the loading of pSiO2 is constant 2.0 phm) which X:the loading of pSiO_2; Y: the loading of nSiO_2.

2.5 Characterization

Fourier transform infrared (FTIR) spectra of polymer were obtained using aNicolet Magna-IR750 scanning range from 4000 to 400 cm^{-1}. The monomer conversion and solid content were calculated gravimetrically. Zeta-potential and size distribution measurements were carried out via using a Malvern zetasizer 3000HSA. Every sample was tested at least 3 runs. TEM analyses were carried out on a JEM 2010, sample was diluted 500-flod by deionized water with ultrasonication and dyed on copper grids before observation. The water contact angles were measured using CAM200 contact angle goniometer, the values reported were the average of three drops per samples at

different locations. The morphology and dispersion of latex-coated SiO_2 were observed with a scanning electron microscope (FESEM, Sirion 200 FEI) at an accelerating voltage of 10 kV. The specimens were dulited in deionized water, casted onto a clean wafer with a 60 °C in oven for 1 h and then selectively coated with gold by a sputter coater before observation. The architecture of composite films were also observed under the SEM. Thermal gravimetric analysis (TGA) was carried out using a Q5000 IR thermal gravimetric analysis from 50-700 °C at a heating rate of 10 °C /min under nitrogen condition.

2.6 Film Formation and Adhesion Testing

180°-peel resistance, T-peel resistance, and shear resistance were measured according to the standards. [29] The latex was filtered using stainless steel filter (30 mesh) and cast onto the standard test panel (304 stainless panel) and aluminum sheet (LY-12CZ) with the help of the self-made coater to make the thickness of dry film 100 ± 30 μm and 300 ± 30 μm. Test strips were made with the help of the steel roller (85 ± 2.5mm in diameter and 45 ± 1.5 mm in width, covered with rubber approximately 6 mm in thickness, having a Shore scale A durometer hardness of 80 ± 5, the surface shall be a true cylinder void of any convex or concave deviations. The mass of the roller is 2040 ± 45 g), The roll coater was passed through the film front to back at least twice (i.e.,along the length of the film). After 24h at room temperature. 12h later multifunction tensile machine (CMT, SANS) was used to evaluate the 180°-peel resistance and T-peel resistance.

Respectively, ASTM D3330 Test Method A (Single-Coated Tapes, Peel Adhesion

at 180°Angle) evaluated peel resistance at a peel angle of 180°. The substrate and the strip were inserted into the grips (C-clamp) and the lower grip was set to move downward at a speed of 300 mm/min. The average force per 25mm required to peel the strip from the substrate was recorded and reported at 180°-peel resistance. ASTM D1876-01 measures T-peel resistance, akin to the test of 180°-peel resistance.

Shear resistance was assessed by tension loading shear test according to ASTM D2294-96. This test consisted in applying a standard area of the tape (25 mm × 12.5 mm) on the steel panel holding in the grips (C-clamp) and the lower grip was set to move downward at a speed of 5 mm/min. All experiments were carried out under the standard conditions (T=23 °C and humidity = 55%)

3. Results and Discussion

3.1 Synthesis of P2EHA-pSiO2 and P2EHA-pSiO2/nSiO2 Composite Particles

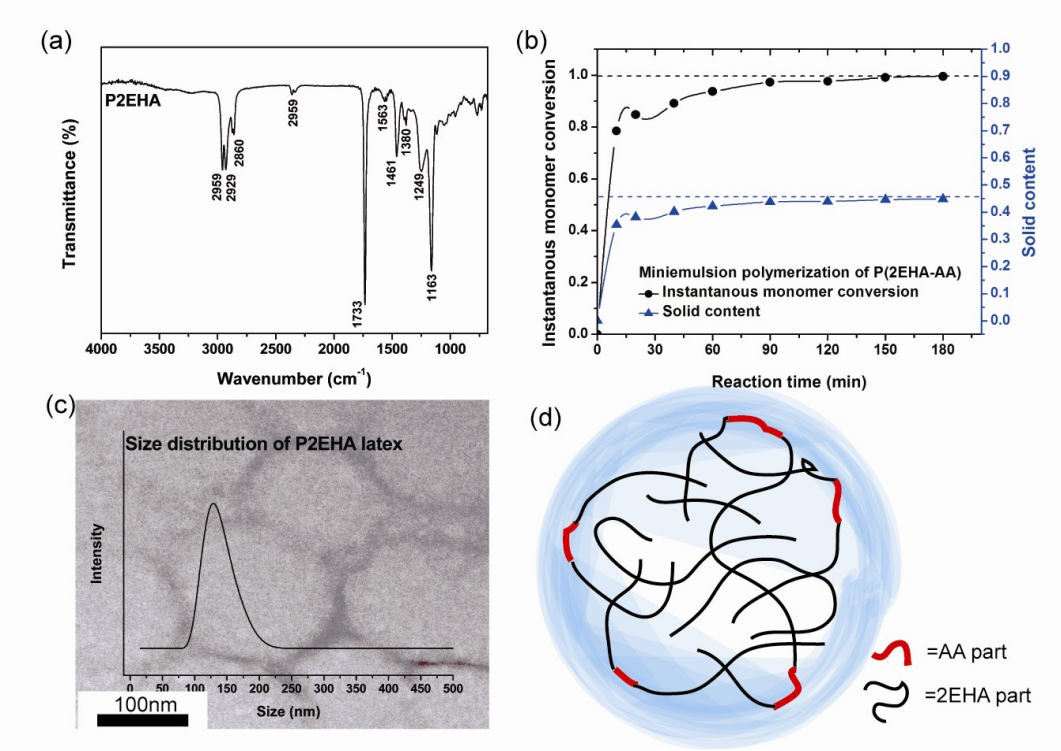

Figure 1. (a) FTIR spetra of P2EHA; (b) Evolution of the instantaneous conversion and

solid content during the miniemulsion polymerization of monomer 2-EHA and AA; (c) TEM image and size distribution of P2EHA particles with scale bar of 100nm; (d) The structure model of P2EHA particle with AA part on the surface.

Figure 1 (a) showed the FTIR spectra of P2EHA. The significant peak at 1733 cm-1 corresponds to C=O, and 1250-1000 cm-1 to C-O group. 1461 cm-1 and 1380 cm-1 suggest the bend vibraton of –CH2 or –CH3. 2959 cm-1 ,2929 cm-1 and 2860 cm-1 are attributed to the stretch vibration of C-H. 2362 cm-1 belongs to the –C≡N group. The characteristic C=C strong adsorption near 1580-1650 cm-1 is absent. Indicating that C=C contained in monomers has almost been reacted completely. Figure 1 (b) presented the process of miniemulsion polymerization of monomer 2-EHA and AA. Because of the existence of oil-soluble initiator (AIBN) in the droplets of monomer miniemulsion, the conversion increase fastly at the first 30min. Then, the reaction rate tends to be stable gradually, belong to the viscosity increase, monomer consumption and the devoid of free radicals. Solids content had a similar trend. We synthesized P2EHA latex particles that contained –COOH group on the surface via a miniemulsion polymerization method with the size of 150 nm(Figure 1 (c)). Carboxylic acid (COOH) groups were hydrophilicity, therefore, acidic monomers tend to concentrate at the particle surface during the emulsion polymerization with the more hydrophobic monomers localized within the particle cores.[30] Figure 1 (d) showed the structure model of P2EHA particle. The particles are charged-stabilized by the presence of carboxyl group at the colloidal surface originating from the monomer acrylic acid.

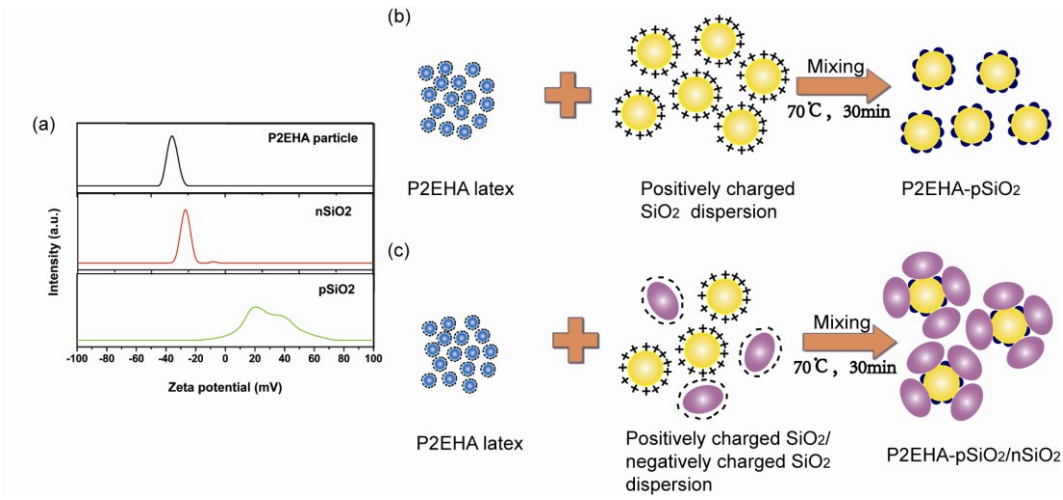

Figure 2. (a) Zeta potential of P2EHA, $nSiO_2$ and $pSiO_2$ particles. (b) Schematic illustration of self-assembly of P2EHA latex and $pSiO_2$, followed by mixing with a suitable temperature and time. (c) Schematic illustration of self-assembly of P2EHA latex and $pSiO_2$/$nSiO_2$, followed by mixing with a suitable temperature and time.

The zeta potential of $pSiO_2$, $nSiO_2$, and P2EHA latex are +30.2 mV, -54.1 mV, and -69.9 mV respectively (showed in Figure 2 (a)). The difference of zeta potential (or surface charge) on the particle surface was ultralized to prepare the composite particles by self-assembly of P2EHA and $pSiO_2$ or $pSiO_2$/ $nSiO_2$ through electrostatic interaction. Figure 2 (b) and Figure 2 (c) showed these processes. Due to the size of $pSiO_2$ particle is about 1 μm, therefore the latex particle will absorb on the surface of $pSiO_2$ particle. Miniemulsion polymerization was an effective method to prepare stable latex particles with around 100nm which was smaller than $pSiO_2$ particles.[31] Therefore more small latex particles would adsorb on the surface of $pSiO_2$ which was benefit to improve the dispersibility and compatibility of SiO_2 in polymer matrix.

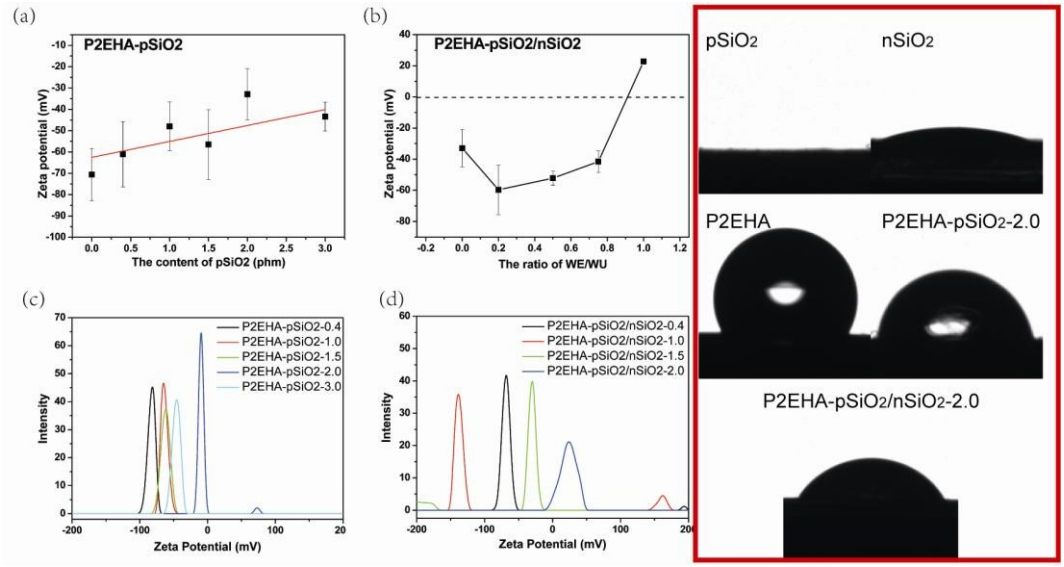

Figure 3. The surface zeta-potential of (a) P2EHA-$pSiO_2$ composite particle. (b) P2EHA -$pSiO_2$/$nSiO_2$ composite particle. Red box: the pictures of water contact angle.

Table 1. The values of water contact angle.

	Values of water contact angle (°)
$pSiO_2$	≈ 0
$nSiO_2$	19.414 ± 0.423
P2EHA	120.543 ± 0.265
P2EHA-$pSiO_2$-2.0	83.213 ± 2.6625
P2EHA-$pSiO_2$/$nSiO_2$-2.0	59.463 ± 1.0465

In order to demonstrate the effective absorption of the polymer latex particles on the $pSiO_2$ surface. Zeta-potential of the composite particles were measured. The uniform distribution of the polymer latex particles over the $pSiO_2$ core is a good indication of a uniform charge distribution of the particles. As we all know in colloidal science, suspensions with absolute zeta potential values higher than 30 mV are

generally considered to be stable.[32] We can find in Figure 3 (a) and (c), the final zeta-potential of P2EHA-pSiO_2 composite particles were measured and yielded the values of < -30mV with single distribution peak , indicating that the surface is now overcharged with negative species, resulting in the observed colloidal stability. The water contact angle of SiO_2, P2EHA and composite materials were showed in Figure 3 red box and Table 1. The hydrophilicity of SiO_2 would reduce compatibility with the polymer matrix which was hydrophobic. Compared to SiO_2, a significantly increasing of water contact angle for the composite materials were observed which proved the adsorption of P2EHA particles on pSiO_2 surface. The reduction of water contact angle when compared P2EHA-pSiO_2/nSiO_2-2.0 to P2EHA-pSiO_2-2.0 also proved the adsorption of nSiO_2 on pSiO_2 surface. TEM analysis yielded the pictures of the composite particles showed in Figure 4 (e) and (f). As can clearly be seen that a significant deformation between composite particles showed in Figure 4 (e) due to the more soft P2EHA particles which adsorbed on pSiO_2 surface. Because of the hard of pSiO_2 particle and small amount of soft P2EHA particles which adsorbed on pSiO_2 surface, we could not observe a significant deformation between composite particles showed in Figure 4 (f). Therefore the pSiO_2 particles are covered with the polymer latex particles and yielded the composite particles. There were no surface charge reversion happened meant that the polymer latex particles absorbed on the surface of pSiO_2 successfully. In addition, the TEM-EDX mapping spectra also showed the adsorption of P2EHA on SiO2 surface (Figure S1). Interestingly, when the loading of pSiO_2 was increased, we found that the charge of the final P2EHA-pSiO_2 composite particle also

increased. This change of the surface charge also reflected the number of polymer latex particle absorbed on the surface of $pSiO_2$ which was an powerful evidence for the film formation mechanism.

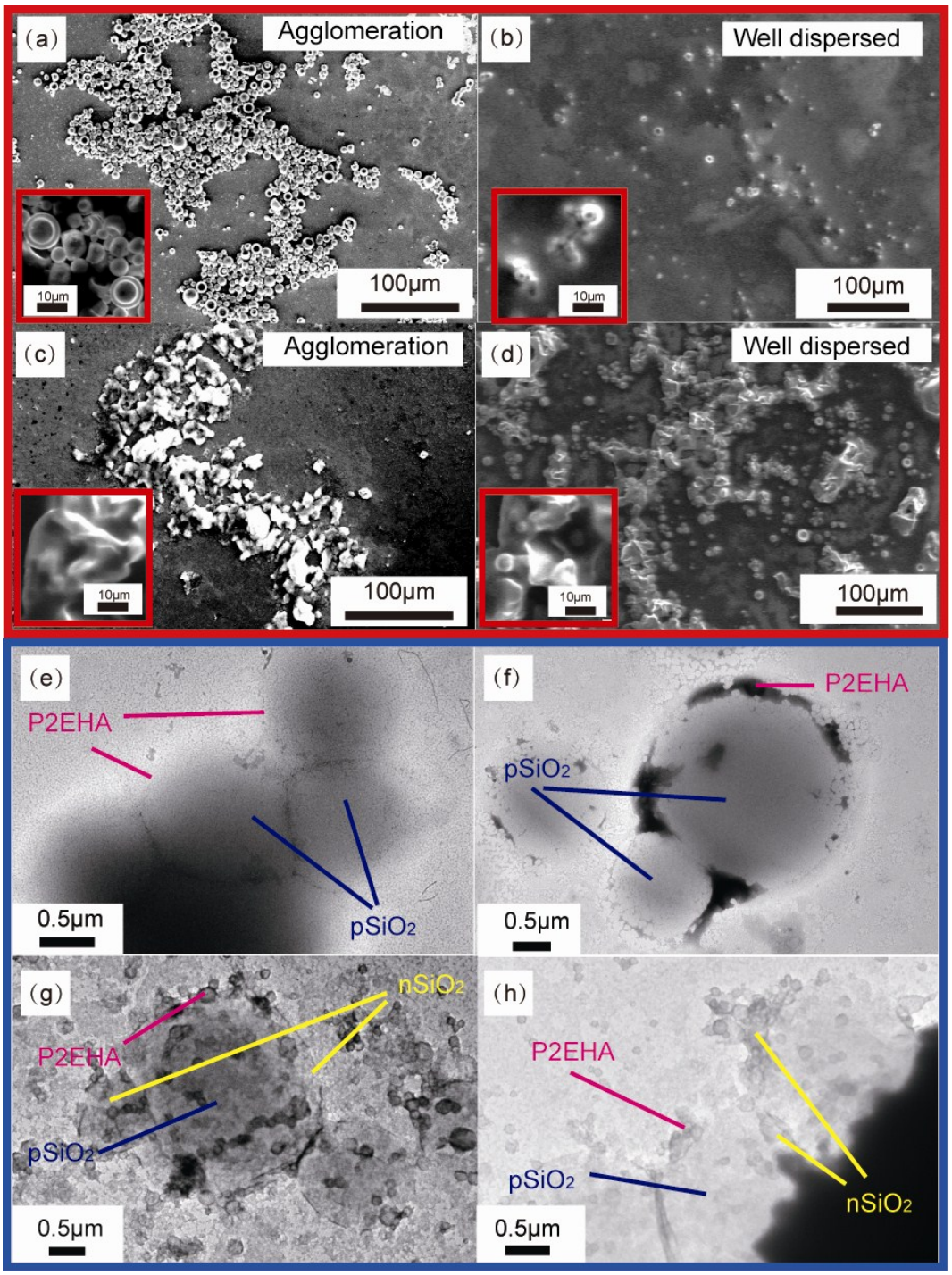

Figure 4. Red box: SEM images of (a) pristine-$pSiO_2$, (b) P2EHA-$pSiO_2$ composite particles (without coating gold), (c) pristine-$nSiO_2$ composite particle, and (d)

p2EHA-pSiO_2/ nSiO_2 composite particles (without coating gold). Blue box: TEM images of (e) P2EHA-pSiO_2-0.4, (f) P2EHA-pSiO_2-2.0, (g) P2EHA-pSiO_2-2.0/nSiO_2-1.0, and (h) P2EHA-pSiO_2-2.0/nSiO_2-0.4 composite particles.

Because of the low Tg (glass transition temperature, -85°C) of P2EHA, we investigated the dispersion of SiO_2 in polymer matrix via scanning electron microscopy without coating gold on the composite film species which the thickness was about 1 mm showed in Figure 4 SEM images. Comparing with the SEM pictures of pristine pSiO_2 and nSiO_2 showed, the mixing with polymer latex particle improved the dispersion and reduced the agglomeration of SiO_2 particle in polymer matrix because of the electrical reversal and excellent compatibility. Once charged SiO_2 met with P2EHA latex particles, strong ionic interactions took place and yielded a new surface charge.

In the experiments with the loading of nSiO_2, the surface zeta potential will decrease dramatically. The absorption of nSiO_2 and latex particle on pSiO_2 surface could be proved by measuring the zeta-potential with the single distribution peak showed in Figure 3 (b) and (d) and the SEM showed in Figure 4 (c) and (d). TEM pictures of this composite particles were showed in Figure 4 (g) and (h). Bucause of the more adsorption of hard nSiO_2 on pSiO_2 surface, there was no significant deformation between composite particles showed in Figure 4 (g). Due to the decrease of hard nSiO_2 particles adsorbed on pSiO_2 surface, we could find deformation but not significant showed in Figure 4 (h). When we increased the loading of nSiO_2, the zeta-potential was increased and still under 0 mV. However, when the ratio of nSiO_2/pSiO_2 above 1, a charge inversion happened. The main reason might be that the excess of nSiO_2 caused

the settlement phenomenon.[33]

Because of the anionic-nonionic mixed emulsifiers used in preparing P2EHA latex, we had to investigate that whether the redistribution of the emulsifiers could also caused the coalescence of SiO_2 and P2EHA particles. Briefly that electrostatic interaction or emulsifiers which one was the main driving force for the adsorption of P2EHA particles on $pSiO_2$ surface. Therefore, we replaced charged SiO_2 by neutral SiO_2 has similar size with pSiO2 showed in Figure S2 SEM image, however, we could not obtain a stable system that neutral SiO_2 agglomerated and settled down to the bottom. The reason might be that the amount of the redistributed anionic-nonionic mixed emulsifiers is too small to maintain the stability of SiO_2 with micrometer. So the main driving force for the adsorption of P2EHA particles on $pSiO_2$ surface was electrostatic interaction.

3.2 The Mechanism of Film Formation

The loading of the fillers led to a dramatic increase in interfacial area as compared with the pure materials. The interfacial area created a significant volume fraction in interfacial polymer with properties different from the bulk polymer even at low content.[34] Uniform distribution of SiO_2 particles as fillers in the matrix played an important role in the mechanical properties and thermo-tolerance performance of P2EHA-SiO_2 composite materials.[35] Due to the results of zeta-potential, we could know that the ratio of P2EHA latex particles and SiO_2 particles would affect the morphology of the P2EHA/ SiO_2 composite particles and then decide the film architecture. In order to link micro and macro, we established the film formation mechanism. Three steps of suspension of composite particles in water, close-packing during drying, and film

formation after drying were presented subsequently.

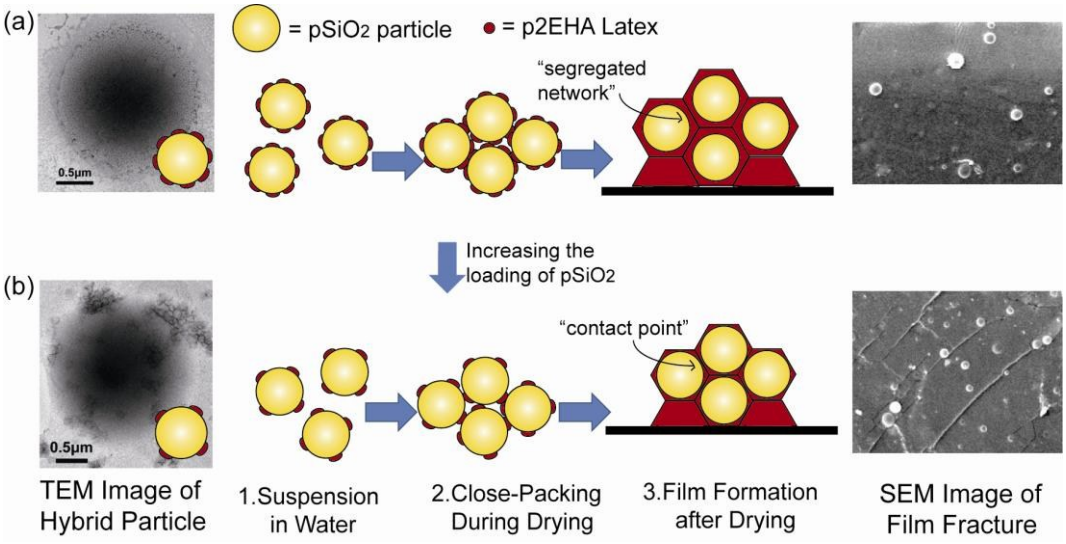

Figure 5. Schematic of film formation for the loading of $pSiO_2$ with TEM images and fracture surface SEM images. Increasing the ratio of $pSiO_2$ particle/polymer latex particle would introduce the architecture of composite film from (a) segregated network to (b) contacted network.

For the two component system of P2EHA and $pSiO_2$. The small loading of $pSiO_2$ introduced to the low ratio of $pSiO_2$ particles/P2EHA latex particles. Therefore, the surface of $pSiO_2$ particles would absorb a mount of P2EHA latex particles. This phenomenon resulted in the segregated network in the composite film materials showed in Figure 5 (a). Smooth surface without cracks showed in the SEM image of Figure 5 (a). When we increased the loading of $pSiO_2$, meant that the high ratio of $pSiO_2$ particles/P2EHA latex particles which reducing the amount of adsorption of P2EHA latex particles on $pSiO_2$ particles surface. The contact point between $pSiO_2$ particles appeared showed in Figure 5 (b). Comparatively, the rougher fractured surface showed in the SEM image of Figure 5 (b) mainly due to the mutual contacting and compression of $pSiO_2$ particles.

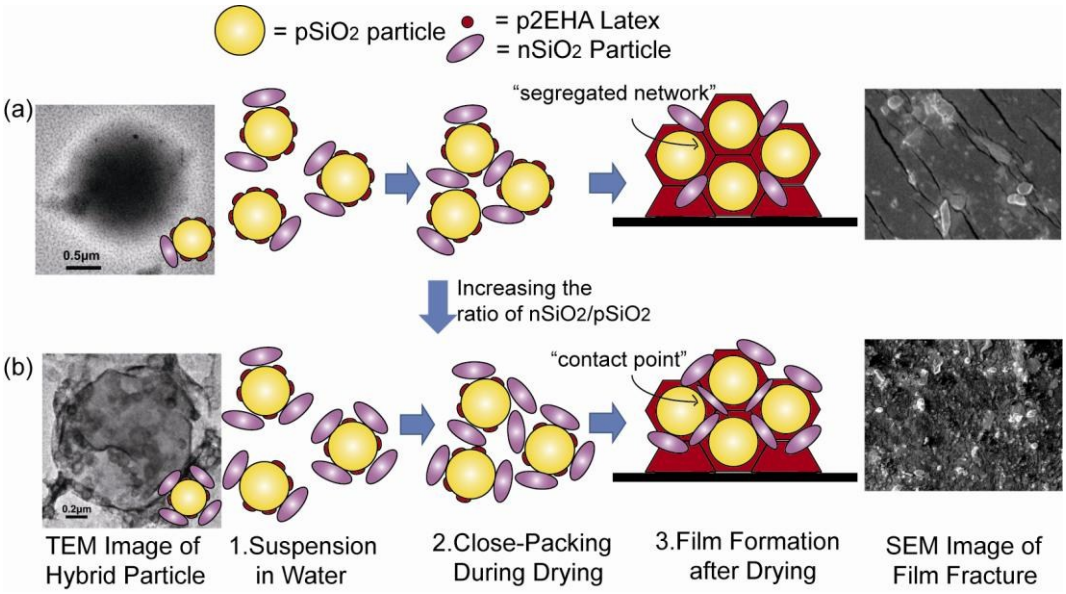

Figure 6. Schematic of film formation for the loading of $pSiO_2$ and $nSiO_2$ with TEM images and fracture surface SEM images. Increasing the ratio of $nSiO_2/pSiO_2$ particle would introduce the architecture of composite film from (a) segregated network to (b) contacted network which the loading of pSiO2 was constant 2.0 phm.

For the three component system of P2EHA, $pSiO_2$, and $nSiO_2$. The content of $pSiO_2$ was constant 2 phm. Due to differences in surface charge of P2EHA, $pSiO_2$, and $nSiO_2$. The ratio of $nSiO_2$ particles and $pSiO_2$ particles would also decide the acrchitecture of P2EHA-$pSiO_2$/$nSiO_2$ composite which was showed in Figure 6. On the basis of P2EHA/$pSiO_2$ film architecture, we could think that the loading $nSiO_2$ would intersperse into polymer matrix between the $pSiO_2$ particles. Low ratio of $nSiO_2/pSiO_2$ would still keep the segregated network in the P2EHA-$pSiO_2$/$nSiO_2$ composite film architecture. Smooth surface but with a few cracks showed in the SEM image of Figure 6 (a). When we incresed the ratio of $nSiO_2/pSiO_2$, The $nSiO_2$ particles would fill into the gap as a "cross-linker" formed the contact point between the $pSiO_2$ particles. The rougher fractured surface showed in the SEM image of Figure 6 (b).

In addition, the TEM image of composite materials showed in Figure 4 blue box was a convincing evidence for the film formation mechanism which showed the relationship between the deformation with the amount of SiO_2.

3.3 Thermal-Tolerance performance of P2EHA-SiO_2 Composite Materials

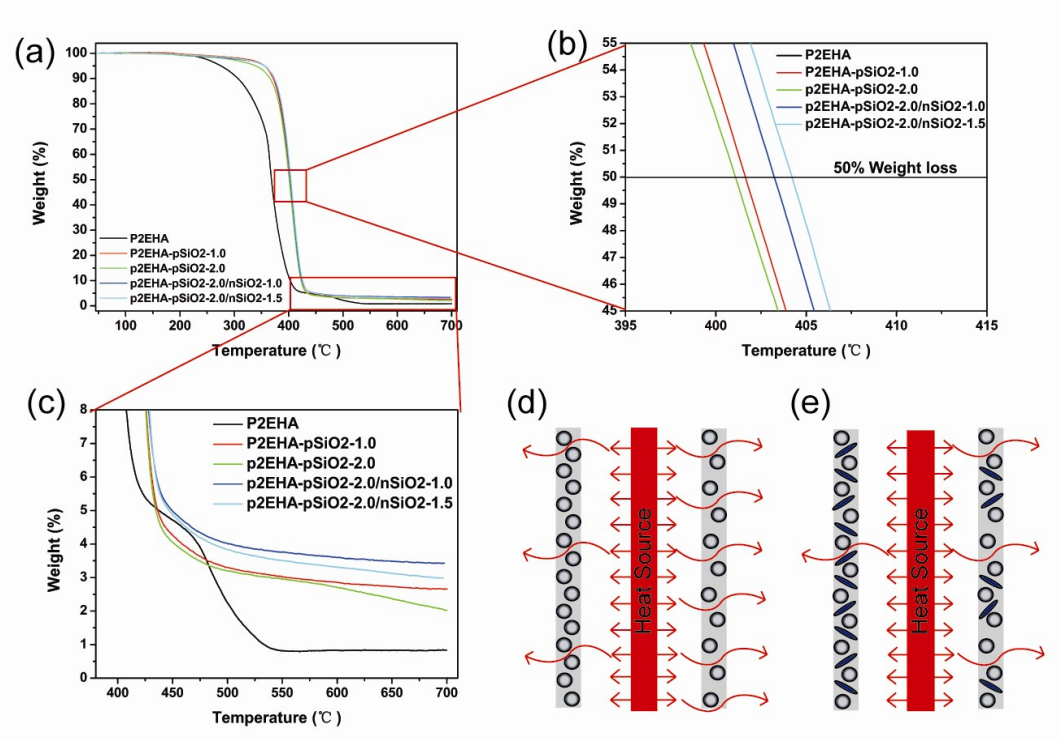

Figure 7. The TGA curves of pure P2EHA latex particles, P2EHA-pSiO_2-1.0, P2EHA-pSiO_2-2.0, P2EHA-pSiO_2-2.0/nSiO_2-1.0, P2EHA-pSiO_2-2.0/nSiO_2-1.5 (a), (b), (c) and the model of composite materials' thermo-tolerance performance of (d) P2EHA-nSiO_2 and (e) P2EHA-nSiO_2/pSiO_2.

Thermal-tolerance performance of P2EHA-pSiO_2 composites and P2EHA-pSiO_2/nSiO_2 composites characterized in nitrogen conditions is shown in Figure 7 (a) and the temperature at 50% weight loss, $T_{50\%}$ occurred are showed in Figure 7 (b). The loading of charged SiO_2 increases the decomposition temperature and reduces the decomposition rate of the polymer composites. The onset decomposition

temperatures of polymer composites are somewhat different, but this difference is not significant. However, they had some tangible influences on $T_{50\%}$, with the P2EHA-pSiO_2/nSiO_2 composites showing about 3-4 °C higher than the P2EHA-pSiO_2 composites.

The improvement in thermal-tolerance performance of P2EHA-SiO_2 composites can be attributed to the formation of the network and tortuous paths in the polymer matrix, which acted as a barrier inhibiting the emission of the decomposition products during combustion showe in Figure 7 (d) and (e).

Figure 7 (c) presented the temperature at about 95% weight loss, the residual weight of P2EHA-pSiO_2-2.0 and P2EHA-pSiO_2-2.0/nSiO_2-1.5 were less than P2EHA-pSiO_2-1.0 and P2EHA-pSiO_2-2.0/nSiO_2-1.0 respectively. The reason might be that, efficient thermal-tolerance caused the detention of heat in the matrix of composite materials, therefore there were enough time to decompose for polymer in the composite materials.

3.4 The Adhesive Properties and Mechanism of P2EHA-SiO_2 Polymer Composite Film

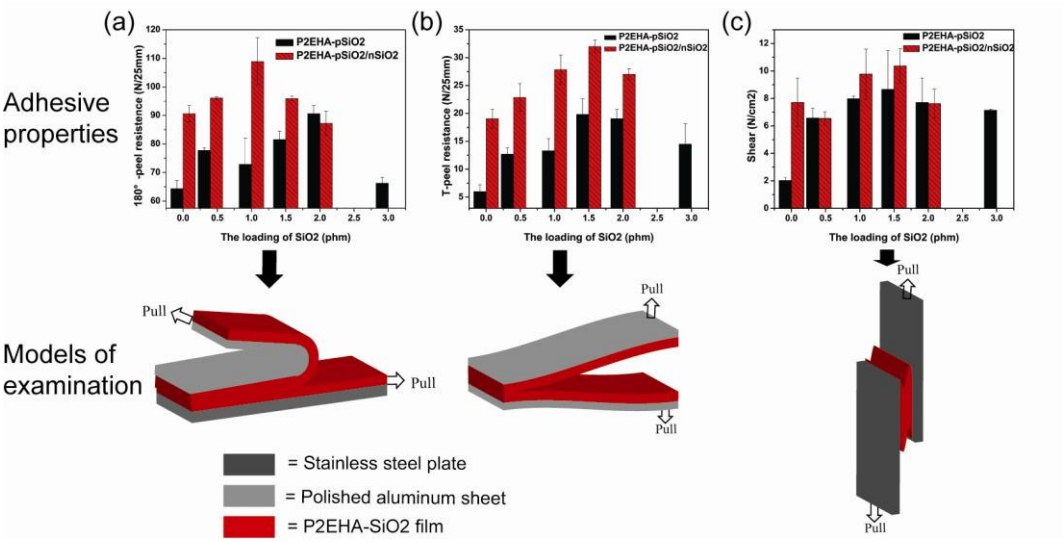

Figure 8. The adhesive properties of (a) 180°-peel resistance, (b) T-peel resistance, and (c) shear resistance which the content of adding meaning the loading of $pSiO_2$. With the models of examination.

Because one of the most common applications of P2EHA was as adhesive,[36, 37] we tested the effect of loading SiO_2 on the adheisve properties of P2EHA. Figure 8 showed the adhesive properties of the P2EHA/SiO_2 composite materials with the models of examination. The 180°-peel resistance, T-peel resistance, and shear resistance showed a decreasing trend after a prior increase that a balance of cohesive resistance and viscoelastic properties was achieved. This trend was similar to the research of Chen[38]. When the concentration of the $pSiO_2$ was 2.0 phm, the 180°-peel resistance reached the maximum for 90.63 N/25mm. When the concentration of the $pSiO_2$ was 1.5 phm, the T-peel resistance and shear resistance reached the maximum for 19.83 N/25mm and 8.66 N/cm^2, respectively.

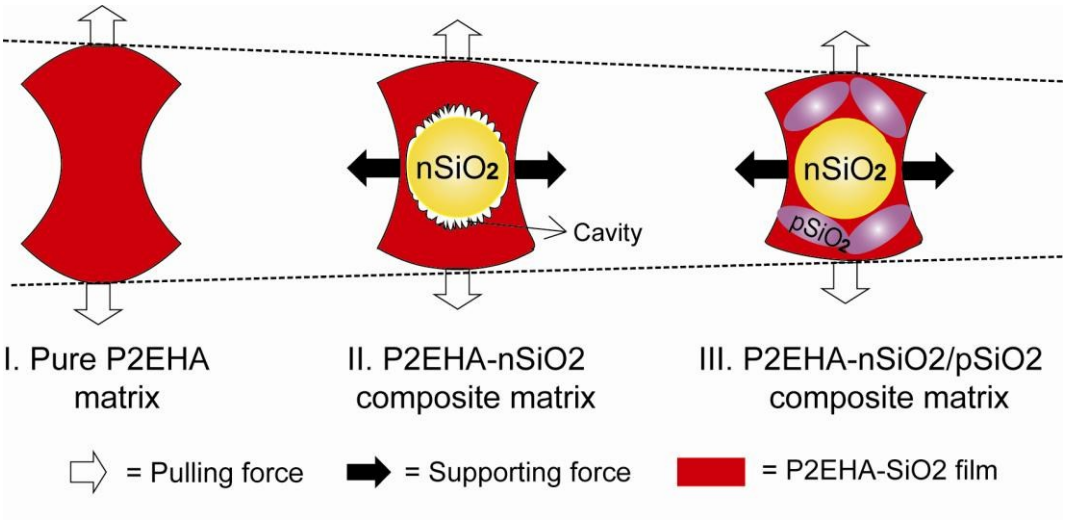

Figure 9. The simplified model of examination.

In order to investigate the influence of SiO_2 on adhesive mechanism of composite film, the models of examination showed in Figure 8 were simplified into the model showed in Figure 9. The reasons might be that the adhesive properties was mostly due to increases in displacement at failure on addition of SiO_2, so under the pulling process showed in Figure 9, the pulling force led to the deformation of the polymer matrix, the supporting force could be found in II. P2EHA-$nSiO_2$ composite matrix and III. P2EHA-$nSiO_2$/$pSiO_2$ composite matrix due to the rigidity of the SiO_2 particles. This process dissipated amounts of energy and resulted in high adhesive resistance.[39] Therefore, we had to put higher pulling force to obtain the same deformation with I. Pure P2EHA matrix. When the concentration of the $nSiO_2$ was 1.0 phm, the 180°-peel resistance reach the maximum for 108.88 N/25mm. As the concentration of the $nSiO_2$ was 1.5 phm, the T-peel resistance and shear resistance reach the maximum for 31.98 N/25mm and 10.37 N/cm^2, respectively. The difference between P2EHA-$nSiO_2$ composites and P2EHA-$nSiO_2$/$pSiO_2$ composites might be that, the loading of $pSiO_2$ could delay or even prevent the cavities (resulted from the weak interaction,

electrostatic force between SiO_2 particles and polymer matrix[4, 40]) formed in II. P2EHA-nSiO_2 composite matrix. Therefore, the higher adhesion and cohesion we could get from the three component system of P2EHA, pSiO_2, and nSiO_2. However, when the SiO_2 content further increased, the adhesive properties became worse. The main reason might be the excess of SiO_2 caused the less adsorption of P2EHA particles on SiO_2 surface and reduced the compatibility with the polymer matrix, then resulted in the settlement and agglomeration phenomenon which reduced the adhesive properties.[33]

4 Conclusion

We reported a simple, environmentally friendly approach for preparing P2EHA-SiO_2 composite materials by self-assembly of negatively charged P2EHA latex particles and charged SiO_2 particles through electrostatic interaction. The P2EHA-SiO_2 composite materials exhibited excellent thermal-tolerance properties and adhesive properties due to the formation of the special architecture in the composite materials which have an application potential for a high effective PSA (pressure sensitive adhesive) which a balance of cohesive resistance and viscoelastic properties was achieved. We belive that this approach can be used for polymer composites not only for P2EHA and SiO_2 but also for several other vinyl polymers which can be prepared via emulsion polymerization by free radical initiators such as polyacrylonitrile (PAN), polystyrene (PS), poly vinyl acetate (PVAc), and poly (vinyl chloride) (PVC) and many other inorganic particles such as titanium dioxide (TiO_2), ferric oxide (Fe_2O_3), nano-gold (Au), nano-silver (Ag).

5 Notes

The authors declare no competing finacial interest.

ACKNOWLEDGEMENT

Senior Engineer Zhaoqin Chu is acknowledged for TEM assistance and Dr. Wei Xu is thanked for the TGA studies from Institute of Solid State Physics, Chinese Academy of Sciences, Hefei 230031, PR China.

References

1. F. Deplace, C. Carelli, A. Langenfeld, M. A. Rabjohns, A. B. Foster, P. A. Lovell and C. Creton, *ACS Appl. Mater. Interfaces*, 2009, **1**, 2021-2029.
2. A. C. Balazs, T. Emrick and T. P. Russell, *Science*, 2006, **314**, 1107-1110.
3. L. S. S. Pulickel M. Ajayan, Paul V. Braun, *Nanocomposite Science and Technology*, Wiley-VCH: Weinheim, Germany, 2003.
4. T. Wang, C. H. Lei, A. B. Dalton, C. Creton, Y. Lin, K. A. S. Fernando, Y. P. Sun, M. Manea, J. M. Asua and J. L. Keddie, *Advanced Materials*, 2006, **18**, 2730-2734.
5. A. M. Pinto, J. Martins, J. A. Moreira, A. M. Mendes and F. D. Magalhães, *Polymer International*, 2013, **62**, 928-935.
6. T. Wang, P. J. Colver, S. A. F. Bon and J. L. Keddie, *Soft Matter*, 2009, **5**, 3842-3849.
7. L. Cheng, A. Liu, S. Peng and H. Duan, *ACS Nano*, 2010, **4**, 6098-6104.
8. J. Song, L. Cheng, A. Liu, J. Yin, M. Kuang and H. Duan, *Journal of the American Chemical Society*, 2011, **133**, 10760-10763.
9. N. Wang, Y. Guo, H. Xu, X. Liu, L. Zhang, X. Qu and L. Zhang, *Journal of Applied Polymer Science*, 2009, **113**, 3113-3124.
10. H.-J. Tsai and Y.-L. Lee, *Langmuir*, 2007, **23**, 12687-12692.
11. J. Machotová, J. Šňupárek, L. Prokůpek, T. Rychlý and P. Vlasák, *Progress in Organic Coatings*, 2008, **63**, 175-181.
12. M. A. S. Melo, S. F. F. Guedes, H. H. K. Xu and L. K. A. Rodrigues, *Trends in Biotechnology*, 2013, **31**, 459-467.
13. B. Fang, L. Peng, Z. Xu and C. Gao, *ACS Nano*, 2015, **9**, 5214-5222.
14. A. Zhuk, R. Mirza and S. Sukhishvili, *ACS Nano*, 2011, **5**, 8790-8799.
15. G. Carotenuto, Y.-S. Her and E. Matijević, *Industrial & Engineering Chemistry Research*, 1996, **35**, 2929-2932.
16. L. L. Beecroft and C. K. Ober, *Chemistry of Materials*, 1997, **9**, 1302-1317.
17. G. Wang, Y. Chen, X. Shen, J. Li, R. Wang, Y. Lu, S. Dai, T. Xu and Q. Nie, *ACS Appl. Mater. Interfaces*, 2014, **6**, 8488-8496.
18. J. M. Asua, *Journal of Polymer Science Part A: Polymer Chemistry*, 2004, **42**, 1025-1041.
19. H. Sardon, L. Irusta, M. J. Fernández-Berridi, M. Lansalot and E. Bourgeat-Lami, *Polymer*, 2010, **51**, 5051-5057.

20. H. J. Naghash and B. Abili, *Progress in Organic Coatings*, 2010, **69**, 486-494.
21. A. Lopez, Y. Reyes, E. Degrandi-Contraires, E. Canetta, C. Creton and J. M. Asua, *Eur. Polym. J.*, 2013, **49**, 1541-1552.
22. Y. Zhu, S. M. Zhang, Y. Hua, H. Zhang and J. D. Chen, *Industrial & Engineering Chemistry Research*, 2014, **53**, 4642-4649.
23. P. J. Colver, C. A. Colard and S. A. Bon, *Journal of the American Chemical Society*, 2008, **130**, 16850-16851.
24. N. Yousefi, X. Sun, X. Lin, X. Shen, J. Jia, B. Zhang, B. Tang, M. Chan and J.-K. Kim, *Advanced Materials*, 2014, **26**, 5480-5487.
25. Z. F. Wu, H. Wang, K. Zheng, M. Xue, P. Cui and X. Y. Tian, *Journal of Physical Chemistry C*, 2012, **116**, 12814-12818.
26. Y. Chen, Y. Wang, H.-B. Zhang, X. Li, C.-X. Gui and Z.-Z. Yu, *Carbon*, 2015, **82**, 67-76.
27. V. H. Pham, T. T. Dang, S. H. Hur, E. J. Kim and J. S. Chung, *ACS Appl. Mater. Interfaces*, 2012, **4**, 2630-2636.
28. A. Noel, J. Faucheu, M. Rieu, J. P. Viricelle and E. Bourgeat-Lami, *Composites Science and Technology*, 2014, **95**, 82-88.
29. M. Kobayashi and A. Takahara, *Polymer Chemistry*, 2013, **4**, 4987-4992.
30. T. Wang, E. Canetta, T. G. Weerakkody, J. L. Keddie and U. Rivas, *ACS Appl. Mater. Interfaces*, 2009, **1**, 631-639.
31. J. Rodrigues and F. J. Schork, *Journal of Applied Polymer Science*, 1997, **66**, 1317-1324.
32. B. G. van Ravensteijn and W. K. Kegel, *Langmuir*, 2014, **30**, 10590-10599.
33. G. Jia-Hu, L. Yu-Cun, C. Tao, J. Su-Ming, M. Hui, Q. Ning, Z. Hua, Y. Tao and H. Wei-Ming, *RSC Advances*, 2015, **5**, 44990-44997.
34. D. W. Schaefer and R. S. Justice, *Macromolecules*, 2007, **40**, 8501-8517.
35. H. Zou, S. Wu and J. Shen, *Chem. Rev*, 2008, **108**, 3893-3957.
36. A. B. Foster, P. A. Lovell and M. A. Rabjohns, *Polymer*, 2009, **50**, 1654-1670.
37. A. Agirre, J. Nase, E. Degrandi, C. Creton and J. M. Asua, *Macromolecules*, 2010, **43**, 8924-8932.
38. J.-J. Chen, C.-F. Zhu, H.-T. Deng, Z.-N. Qin and Y.-Q. Bai, *J Polym Res*, 2009, **16**, 375-380.
39. U. Khan, P. May, H. Porwal, K. Nawaz and J. N. Coleman, *ACS Appl. Mater. Interfaces*, 2013, **5**, 1423-1428.
40. F. Caruso, H. Lichtenfeld, M. Giersig and H. Möhwald, *Journal of the American Chemical Society*, 1998, **120**, 8523-8524.

TOC

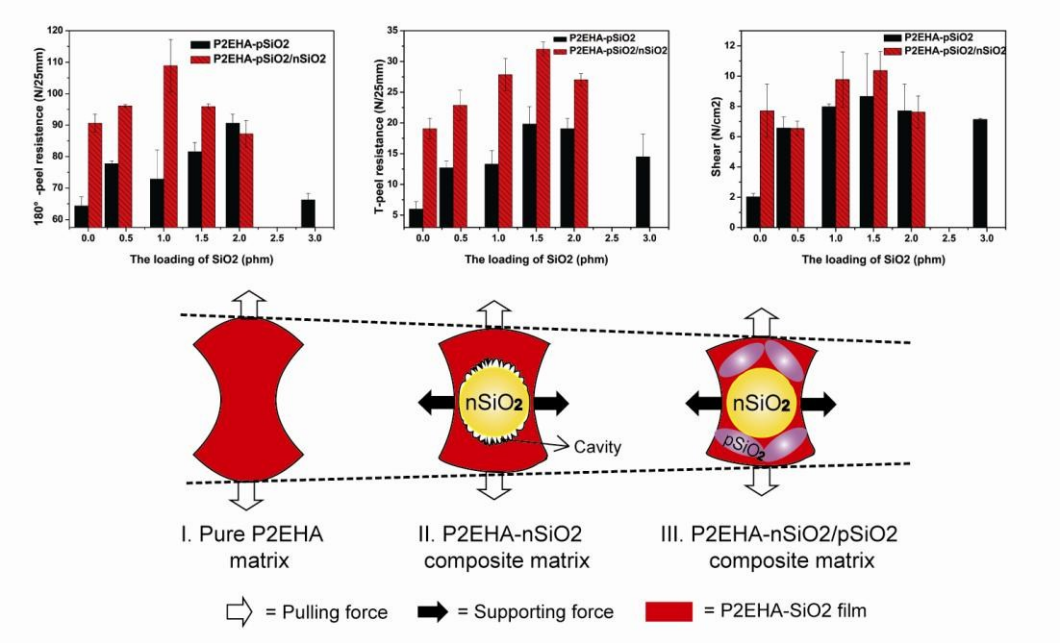

A balance of cohesive resistance and viscoelastic properties was achieved for the P2EHA-SiO2 composites via the loading of charged SiO2.